Comparative study to analyze deformation/fracture behavior under high-velocity impact using different dynamic transient operators

Yogeshwar Jasra[1], Pardeep Kumar[2], Nikesh K Ojha[3] and *†Ravinder K. Saxena[4]

[1,3,4]Department of Mechanical Engineering, Sant Longowal Institute of Engineering and Technology, India.
[2]R V Industries, India

*Presenting author: rks@sliet.ac.in
†Corresponding author: rks@sliet.ac.in

Abstract

Impact and dynamic fracture behavior studies in the structures always hold importance in many areas of science and everyday phenomenon. A process of fracture phenomenon and mechanics of blunt-shaped projectile moving at a high impact velocity will result in fragmentation due to dynamic stress loading also known as the classical Taylor rod impact problem. The present investigation demonstrates the deformation behavior of the flat-faced Taylor rod using different "Direct Integration Schemes" viz. Single/Multi step Houbolt, Newmark beta, Generalized Alpha, etc. under implicit transient dynamic operator and central difference under explicit operator. The finite element analysis is performed using MSC Marc Mentat™. It is further added the plasticity model is incorporated as a Fortran routine in MSC Marc. It is found that instability in the algorithm and irregular deformation can occur using the Newmark Beta scheme. It is also found that the results can be overpredicted using a multi-step Houbolt operator due to high numerical dissipation and the Generalized-alpha method has been presented as an unconditionally stable that allows controllable numerical dissipation and the deformation consistent with experimental results.

Keywords: Computational Mechanics, Finite Element Analysis, Dynamic transient operators, Taylor Rod, Newmark Beta, Houbolt, Generalized Alpha.

Introduction

In the Taylor Rod impact problem, a flat deformable projectile is fired against a fixed rigid target. The experiment is generally used to determine the dynamic yield stresses in the material. It is also performed to validate the constitutive model by comparing the numerical model with the experiments. Taylor [1] was the first researcher who analytically determined the dynamic yield stress by firing the blunt-nosed deformable projectile against the rigid wall. In the study, the mechanical response was determined for the problem involving large plastic deformations, high strain rate, and elevated temperatures. The mathematical model is generally formulated using equations of motion and these equations are solved with the finite element technique (FE) to obtain the solution. The FE formulation of the equation of motion for a dynamic system will result in the ordinary differential equations. A few numerical procedures are available in the literature to solve such coupled differential equations [2]-[7]. The solution is obtained by discretization of the time variable in time intervals. The various functions are assumed to predict the variation in displacement, velocity, and acceleration. The dynamic equilibrium is obtained in the discrete-time increment. So, the numerical methods generally used for solving governing equations of a dynamic system are known as direct integration numerical procedures. Direct integration can be performed in two different ways (Explicit and Implicit). In the explicit integration scheme, the current configuration (t) of the body is known and used to predict the deformed configuration at a time ($t + \triangle t$), In the

implicit integration scheme, the current configuration and the deformed configuration or the dynamic states at both time intervals t and $t + \triangle t$ are required to obtain the solution. In the finite element simulations, the dynamic state at deformed configuration is obtained by the iterative scheme. This procedure is for both linear and nonlinear problems and includes geometric, material, and boundary nonlinearities. The stability and accuracy of the direct integration schemes are determined by the quality of the solutions like in a conditionally stable method the error remains within the prescribed tolerance. The direct integration schemes are in general imprecise. Each integration scheme has various problems like the high-frequency numerical dissipation improves the overall convergence but an uncontrollable numerical dissipation in high-frequency modes can damp out the response in low-frequency mode, but it overall reduces the quality by incorporating the excessive artificial numerical damping in the system.

Woodward et al. [8] performed the two-dimensional axisymmetric finite element simulation and predicted the failure mechanics using an explicit time integration scheme. Worwick et al. [9] analyzed the initiation and propagation of voids in brass. The 2D axis-symmetric analysis was performed using an explicit time integration scheme. Addessio et al. [10] performed the Taylor rod impact simulation using an explicit finite element solver and analyzed the evolution of confined fracture during an impact test. Celentano et al. [11] analyzed the coupled thermomechanical analysis of the Taylor rod. The integration of the time derivative terms was performed using Hilber- Hughes-Taylor (HHT) method. The parameters were chosen using the midpoint rule algorithm. The results were compared with the experimental literature available. Teng et al. [12] determined the fracture patterns in the Taylor rod at the velocity of 600 m/sec. An explicit integration scheme was used to determine the dynamic behavior and fracture pattern. Bao and Wierzbicki [13] analyzed the failure of the target material impacted by a blunt-shaped projectile. The dynamic equations are solved using an explicit time integration scheme. The analysis also suggested that the damage increment is computed only when the triaxiality is greater than -1/3 or, the material is under the tensile loading. This phenomenon has also been introduced in the present study in both implicit and explicit integration schemes. Gautam et al. [14]-[16] predicted the ductile fracture in the Taylor rod impact problem. In the study, Newmark's algorithm is implemented for the implicit integration scheme and algorithmic damping was introduced so to maintain the stability of the solution and to improve the overall response of the system. Rathore et al. [17] analyzed the impact phenomenon by comparing the effect of contact constraints on the overall failure of the target body. In the study, two contact constraints were compared. The dynamic equations were solved using the Newmark integration scheme. Xiao et al. [18] determined the effect of lode parameters in the fracture pattern of the Aluminum alloy Taylor rods. In the analysis, an explicit time integration scheme was implemented to determine the effect of lode angle in the Taylor rod.

It is known that the deformation in the Taylor rod will happen if it impacts the rigid surface at a high velocity. The deformation behavior will depend upon the formulated mathematical model as well as the solution techniques used to solve the model. It will also depend upon the assumed displacement field and the choice of the direct integration schemes in the simulation. Studies are available in the literature which analyze the deformation and fracture behavior of the Taylor rod. Most of the studies used explicit time integration schemes to solve the response of the dynamic system [10] [12] 13] [18]. A very few studies were found in the literature which used the implicit time integration schemes [11] [14-16]. Although, the number of schemes is available and used by the researchers to predict the response of the dynamic system, the effect of different numerical integration schemes on the deformation,

mushrooming and stress distribution in the Taylor rod test appears to be lacking in the literature. So, the objective of the present study is to formulate the finite element model and analyze the deformation in the Taylor rod impact problem using different dynamic transient operators. The investigation will demonstrate the deformation behavior of the flat-faced Taylor rod using different direct integration schemes (Single/Multi step Houbolt, Newmark beta, Generalized Alpha) under an implicit transient dynamic operator. The effect of the Explicit time integration schemes on the deformation behavior has also been analyzed in the present study.

Finite element modeling

Computational model

In the classical Taylor rod impact problem, the flat-nosed projectile is impacted onto a rigid surface. The cylindrical projectile geometric dimensions are presented in Fig. 1. The material parameters are presented in Table 1. The friction coefficient is assumed to be 0.1. Different implicit and explicit direct integration schemes are used to simulate the deformations and fracture pattern of the Taylor rod. The contact between two surfaces is implemented using node to contact segment [17]. The iterative penetration algorithm available MSC Marc Mentat™ [20] is applied to avoid penetration during the impact process. The one-fourth finite element model is simulated using eight noded, brick elements with reduced integration due to symmetry.

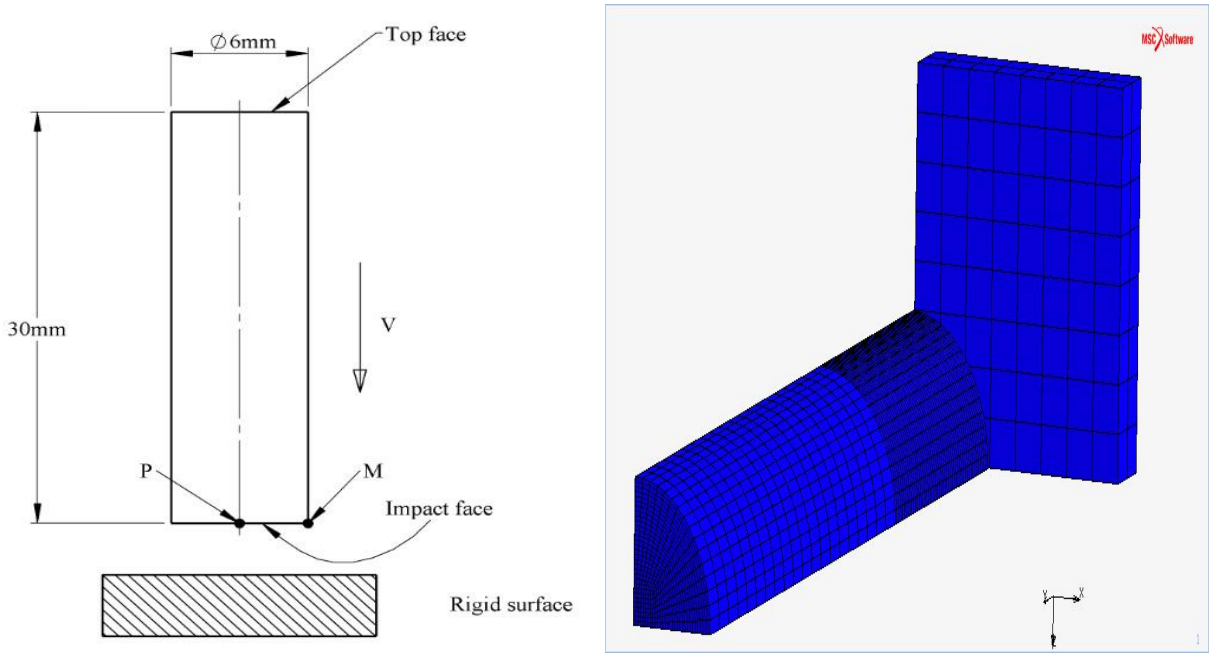

Fig.1 (a). Schematic of Taylor rod impact problem. (b). Finite Element Model of the Taylor rod impact problem.

A fine mesh is modeled in the front part as it involves high deformation and non-linear behavior. It is also expected that the failure will initiate from the front portion of the Taylor rod, therefore, number of elements in the front portion is more as compared to the rear portion of the Taylor rod.

The projectile velocity is taken as 400 m/sec in the simulation to capture the fracture deformation of the Taylor rod. The target is assumed to be much stiffer as compared to the

Property	Notations	Value
Young's modulus	E (N/m^2)	203 x 10^9
Poisson's ratio	υ	0.33
Density	ρ	7850
Initial yield	A (N/m^2)	304.330 x10^6
Strain hardening constant	B (N/m^2)	422.007 x 10^6
Strain hardening exponent	n	0.345
Viscous effect	C	0.0156
Thermal softening constant	m	0.87
Reference strain rate	ε_0	0.0001s^{-1}
Melting temperature	θ_{melt} (K)	1800
Transition temperature	$\theta_{transition}$ (K)	293

Table 1. Material parameters for the mild steel [19]

projectile The projectile rebounds back from the rigid surface after the completion of the impact process.

Material Constitutive Model

The Johnson-Cook (JC) material model is implemented in the MSC Marc Mentat™ in all the direct integration schemes. In the model, the dynamic equivalent stress depends upon the equivalent plastic strain, equivalent plastic strain rate, and temperature. The material is assumed to be elastic up to the initial yield of the material then behaves according to the following relation of the JC plasticity model [21].

$$\sigma = \left[A + B\left(\varepsilon_{eq}^{p}\right)^{n} \right]\left[1 + C\ln\left(\frac{\dot{\varepsilon}}{\dot{\varepsilon}_0}\right)\right]\left[1-\left(T^*\right)^{m}\right] \quad (1)$$

where σ is the equivalent stress, ε_{eq}^{p} is the equivalent plastic strain, A, B, n, C and m are the constants, ε_o is the reference strain rate and T^* is expressed as

$$T^* = \frac{T - T_r}{T_m - T_r}$$

in which T_r and T_m are reference temperature and melting point temperatures. The first bracket represents the quasi-static stress-strain relationship at room temperature, the second term represents the strain-rate hardening, the third term represents the effect of temperature on the plastic behavior of the material. The JC plasticity parameters for the mild steel are listed in Table 1.

Formulation of Direct Integration Schemes

The dynamic equation of motion for the structural analysis is

$$\mathrm{Ma} + \mathrm{Cv} + \mathrm{Ku} = \mathrm{F} \quad (2)$$

where M represents the mass matrix, C is the damping matrix and K is the stiffness matrix. The acceleration is represented by "a", "v" is the velocity, "u" is the displacement and F is the external force vector. There are different integration schemes available in the literature to integrate the equation of motions and to obtain the dynamic response of the system.

Newmark-beta operator

The general form of Newmark beta is represented as [20]

$$u^{n+1} = u^n + \Delta t v^n + \left(\frac{1}{2} - \beta\right)\Delta t^2 a^n + \beta \Delta t^2 a^{n+1} \quad (3)$$

The superscript n represents the n^{th} finite time increment. u is the displacement; v is velocity and a is acceleration.

$$v^{n+1} = v^n + (1 - \Upsilon)\Delta t a^n + \Upsilon \Delta t a^{n+1} \quad (4)$$

If $\gamma = ½$, $ß = ¼$

The equations become

$$\left(\frac{4}{\Delta t^2}M + \frac{2}{\Delta t}C + K\right)\Delta u = F^{n+1} - R^n + M\left(a^n + \frac{4}{\Delta t}v^n\right) + Cv^n \quad (5)$$

where R is the internal force.

$$R = \int_v \beta^T \sigma dv$$

After solving the equations implicitly, the solution of the dynamic system becomes

$$u^{n+1} = u^n + \Delta u \quad (6)$$

Houbolt operator

The velocity and acceleration functions of the Houbolt operator are detailed. The Houbolt operator [20] uses the last three values and by cubic fitting obtain the following expression:

For velocity

$$v^{n+1} = \left(\frac{11}{6}u^{n+1} - 3u^n + \frac{3}{2}u^{n-1} - \frac{1}{3}u^{n-2}\right)/\Delta t \quad (7)$$

For acceleration

$$a^{n+1} = (2u^{n+1} - 5u^n + 4u^{n-1} - u^{n-2})/\Delta t^2 \quad (8)$$

By substituting this expression in the equations of motion

$$\left(\frac{2}{\Delta t^2}M + \frac{11}{6\Delta t}C + K\right)\Delta u = F^{n+1} - R^n + \frac{1}{\Delta t^2}(3u^n - 4u^{n-1} + u^{n-2})M + \frac{1}{\Delta t}\left(\frac{7}{6}u^n - \frac{3}{2}u^{n-1} + \frac{1}{3}u^{n-2}\right)C \quad (9)$$

By solving the equation implicitly and Δu is obtained by using the value from the previous two increments.

Single-Step Houbolt operator

In comparison to the standard Houbolt operator, the single-step Houbolt operator contain few terms related to the beginning of the increment. [20]

$$\alpha^{m1}Ma^{n+1} + \alpha^{c1}Cv^{n+1} + \alpha^{k1}Ku^{n+1} + \alpha^{m}Ma^{n} + \alpha^{c}Cv^{n} + \alpha^{k}Ku^{n} = \alpha^{f1}F^{n+1} + a^{f}F^{n}$$

$$u^{n+1} = u^{n} + \Delta t v^{n} + \beta \Delta t^{2} a^{n} + \beta^{1} \Delta t^{2} a^{n+1}$$

$$v^{n+1} = v^{n} + \Upsilon \Delta t a^{n} + \Upsilon^{1} \Delta t a^{n+1} \tag{10}$$

To solve the equations few assumptions were made to reduce all the unknown parameters into two.

$$\alpha^{k} = 0, \beta = \gamma, \beta^{'} = \gamma + \gamma^{'}, \alpha^{m} = -1/2, \alpha^{k1} = 1/2\beta^{1}$$
$$\alpha^{c} = -(2\beta + \beta')/4(\beta')^{2}, \alpha^{c1} = (2\beta + 3\beta')/4(\beta^{1})^{2}, \alpha^{f} = \alpha^{k}, \alpha^{f1} = \alpha^{k1} \tag{11}$$

Later based on the Taylor series expansion of the displacement function.

$$\beta + \beta' = 1/2$$
$$\gamma = 1/2(1/2 - \gamma')$$

By substituting the velocity and acceleration functions into the equilibrium equations will result in the following simplified form

$$\left\{\frac{1}{\beta^{1}\Delta t^{2}\alpha^{k1}}M + \frac{\alpha^{c1}\Upsilon^{1}}{\beta^{1}\Delta t\alpha^{k1}}C + K\right\}\Delta u = F^{n+1} - Ku^{n} + \frac{1}{\beta^{1}\Delta t^{2}\alpha^{k1}}M\{\Delta t v^{n} + \beta \Delta t^{2} a^{n}\} - \frac{\alpha^{m}}{\alpha^{k1}}Ma^{n} - \frac{\alpha_{c1}}{\alpha^{k1}}C\left\{v^{n} + \Upsilon \Delta t a^{n} - \frac{\Upsilon^{1}}{\beta^{1}\Delta t}\{\Delta t v_{n} + \beta \Delta t^{2} a_{n}\}\right\} - \frac{\alpha^{c}}{\alpha^{k1}}Cv^{n} \tag{12}$$

After solving the equations implicitly, the solution of the dynamic system becomes
$u^{n+1} = u^{n} + \Delta u$

Generalized Alpha Operator

From the equations of motion, the equilibrium equations for the generalized alpha can be expressed in the form [20]

$$M_{a}^{n+1+\alpha_{m}} + C_{v}^{n+1+\alpha_{f}} + K_{u}^{n+1+\alpha_{f}} = F^{n+1+\alpha_{f}}$$

where

$$u^{n+1+\alpha_{f}} = (1 + \alpha_{f})u^{n+1} - \alpha_{f}u^{n}$$

$$v^{n+1+\alpha_{f}} = (1 + \alpha_{f})v^{n+1} - \alpha_{f}v^{n}$$

$$a^{n+1+\alpha_m} = (1+\alpha_m)a^{n+1} - \alpha_m a^n \tag{13}$$

The displacement and velocity functions are similar to the Newmark's functions:

$$u^{n+1} = u^n + \Delta t v^n + \left(\frac{1}{2} - \beta\right)\Delta t^2 a^n + \beta \Delta t^2 a^{n+1}$$
$$v^{n+1} = v^n + (1-\Upsilon)\Delta t a^n + \Upsilon \Delta t a^{n+1} \tag{14}$$

As shown in the literature, the optimized values for the parameters β and γ are related by the following expressions.

$$\beta = \frac{1}{4}(1+\alpha_m - \alpha_f)^2$$

$$\Upsilon = \frac{1}{2} + \alpha_m - \alpha_f \tag{15}$$

If the values for the α_f and α_m are set to zero, then the Generalized alpha equations become equivalent to the Newmark-beta scheme. If the values are varied from $\alpha_m = 0$ and $-0.33 \leq \alpha_f \leq .0$ then the equations become equivalent to HHT method and if the values for the parameters varied from $\alpha_f = 0$ and $0 \leq \alpha_m \leq .1$, it gives rise to the WBZ method. The values of α_f and α_m are related to the behavior of the dynamic system. These parameters are also used to restrict numerical dissipation. Numerical dissipation is related inversely to the spectral radius. The values of α_f and α_m in the MSC Marc Mentat™ FE package can be varied in terms of spectral radius. The relations between the spectral radius and α_f and α_m are presented as:

$$\alpha_f = -\frac{S}{1+S}$$

$$\alpha_m = \frac{1-2S}{1+S} \tag{16}$$

Central Difference Operator

In the central difference operator, the displacement is assumed to vary quadratically over the finite time interval. The following equations are used to describe the variation of displacement over time.

$$a^n = (v^{n+\frac{1}{2}} - v^{n-\frac{1}{2}})/(\Delta t)$$

$$v^n = (u^{n+\frac{1}{2}} - u^{n-\frac{1}{2}})/(\Delta t)$$

$$a^n = (\Delta u^{n+1} - \Delta u^n)/(\Delta t^2) \tag{17}$$

where the incremental displacement is,

$$\Delta u^n = u^n - u^{n-1}$$

$$\frac{M}{\Delta t^2}\Delta u^{n+1} = F^n - R^n + \frac{M}{\Delta t^2}\Delta u^n \tag{18}$$

In the explicit central difference operator, the inverse operation of the matrix is not involved in the explicit analysis.

Results and Discussions

The 3D, high-velocity large deformation analysis of the Taylor test is performed. The constant material properties are assumed in the analysis. The finite element formulation is validated with experimental and numerical results of Celentano et al [11]. It is observed that after impact, the stress wave travel from the outer edge of the projectile towards the central axis of the projectile. Initial elastic wave followed by the plastic wave evolved during the impact in the initial stages using all the direct integration schemes. Initially, i.e., before 2 μs of the impact, mushroom-like deformation of the projectile is observed in the cylinder. Later, the material at the center of the impacting cylinder rebounds in-between 2 to 5μs while the outer edge of the cylinder remains in contact with the target in all the different integration schemes. The deformation process using different integration schemes has been presented in Fig. 3 at different time intervals. This observation of deformation is consistent with Celentano [11]. The stress at the outer surface grows at a higher rate as compared to the central axis of the cylinder due to the large deformation at the outer edge. The von Mises stress contours at different time intervals using different integration schemes have been presented in Figs. 3, 4, and 5. Initially, the standard values of the direct integration schemes have been chosen while analyzing the effect of different integration schemes on the deformation process. The standard values have been taken from the literature. Then these constant values have been varied within well-defined ranges reported in the literature. The overall effect of the variation of the constant parameters on the deformation process of the Taylor rod has also been presented in the following sections. Six different types of dynamic operators (Explicit, Newmark-Beta operator, Wood-Bossak-Zienkiewicz (WBZ)-α modification, Generalized Alpha, multistep Houbolt operator, and the single-step Houbolt operator) are used to analyze the effect of different dynamic operators on the deformation process of the Taylor rod impact problem. Different constant values for these dynamic operators are used in the present work as recommended in the literature. The different values used are presented in Table 2. There are no parameters in the Explicit and Multistep Houbolt operators. The response of the solution depends upon the time step in the case of the multistep Houbolt operator and independent in the Explicit operator.

Validations

The impact test of the flat-ended cylindrical projectile against the rigid wall is performed and validated with the literature available [11]. Figure 1 represents the initial geometry of the projectile. The material properties are taken from the literature [11] for validation. Due to

	Dynamic Operator	Constant Parameter 1	Constant Parameter2
1	Newmark-Beta	$\beta = 0.5$	$\gamma = 0.9142$
2	WBZ	$\alpha_f = 0$	$0 \leq \alpha_m \leq .1$ $\alpha_m = 0.5$
3	Genralized aplha	Spectral Radius 0, $\alpha_f = 0$	$0 \leq \alpha_m \leq .1$, $\alpha_m = 1$
4	Multistep Houbolt	Time step 5e-9	nil
5	Single Step Houbolt	$\gamma' = 1.5$	$\gamma = -0.5$
6	Explicit	Time step 4e-9	nil

Table 2 The constant parameters in different dynamic transient operators

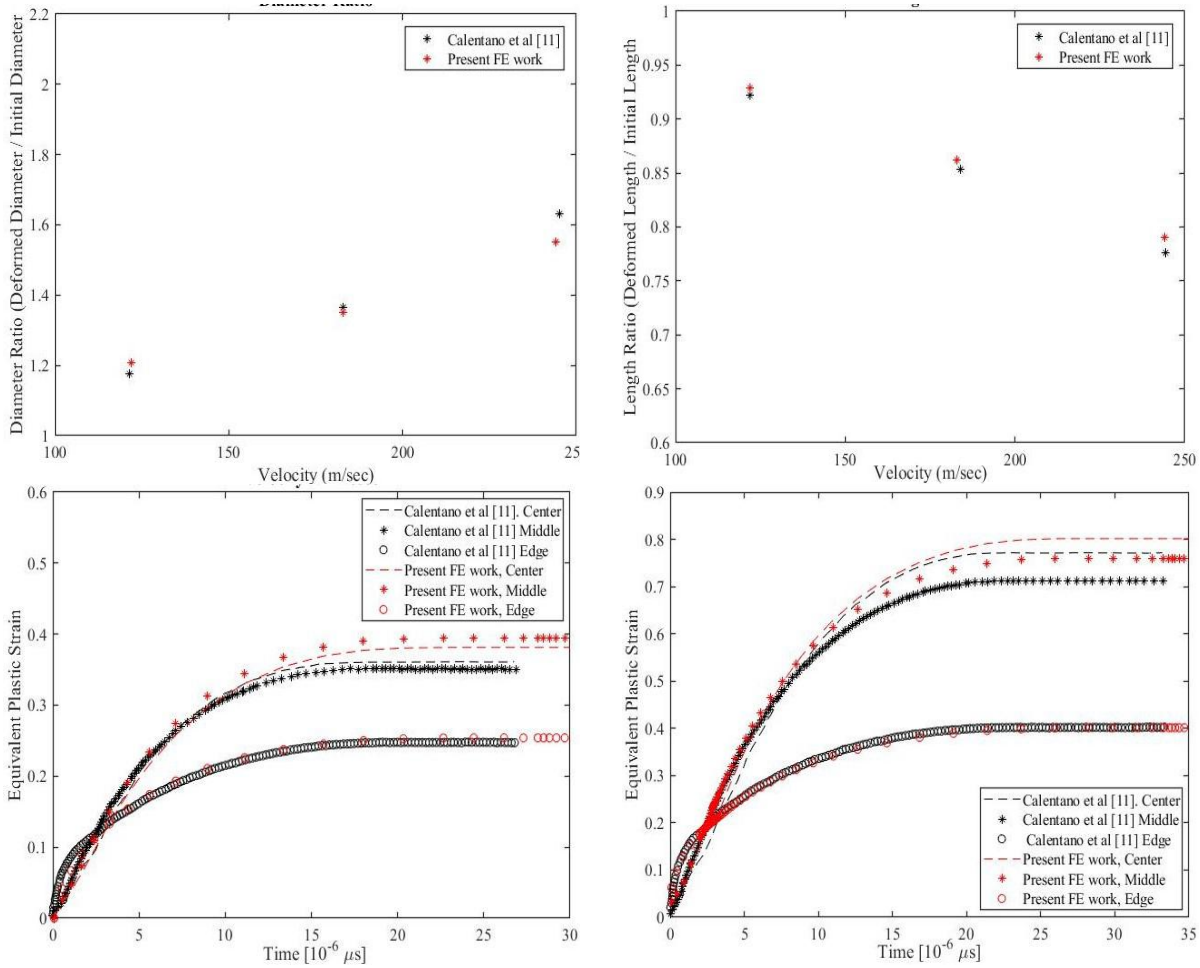

Figure 2. The variation of different characteristics with velocity.

symmetry of the problem, only one-fourth model is considered for the analysis. The heat transfer to the surrounding environment is assumed to be negligible because of the short duration of impact. The predicted result in Fig. 2 is consistent with the literature [11].

Deformation pattern in Taylor rod

The von-Mises stress distribution at three different time intervals has been presented in the section. The first-time interval represents the stress distribution during the mushrooming process just after the initiation of the impact process and at the starting time of the lifting of the central axis reported in the study [16]. The second time step is chosen when the central axis again comes in contact with the target i.e., around 5 to 7 µs. The overall effect of the different integration schemes on the jump of the central point has also been presented in the present study.

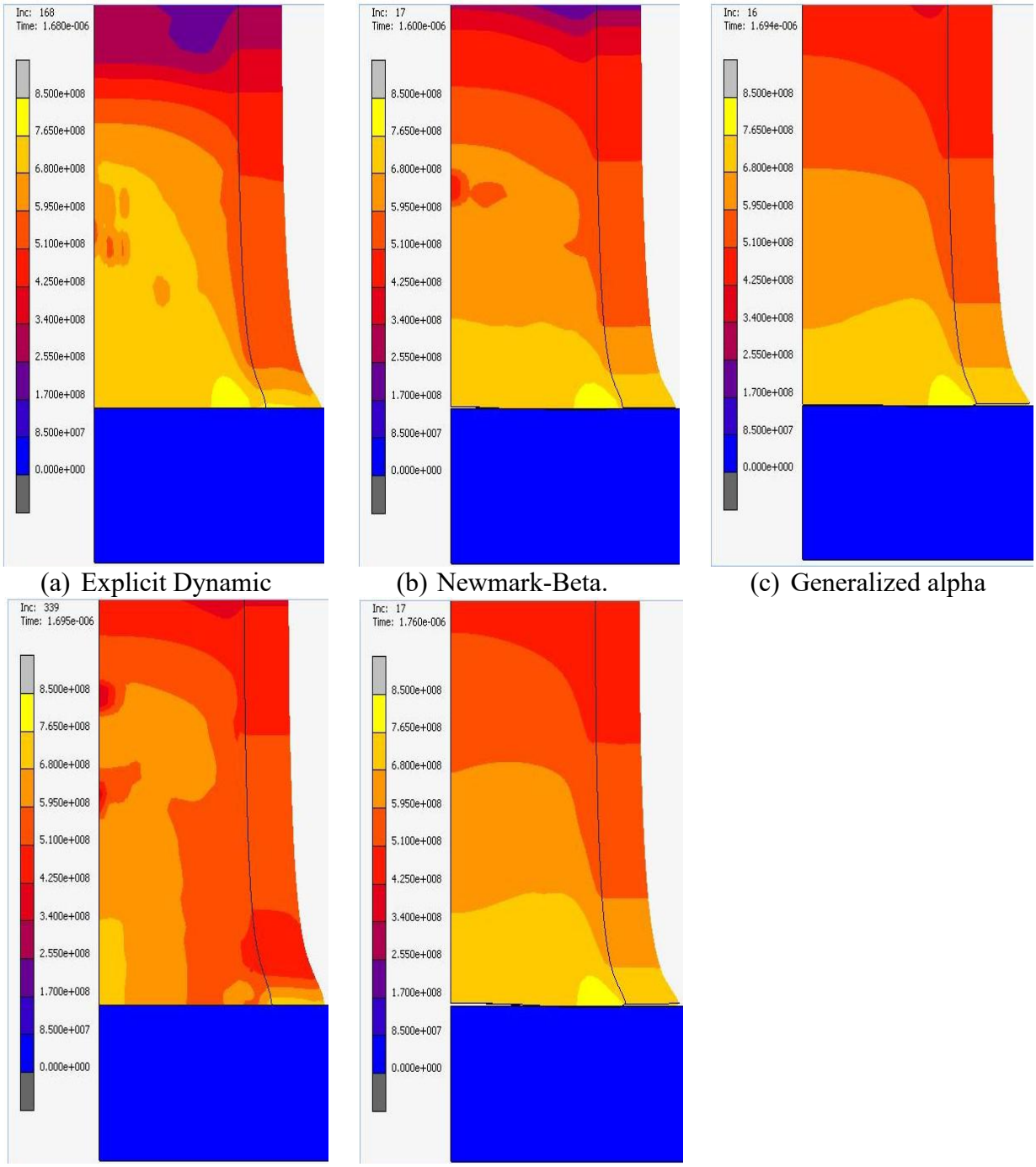

(a) Explicit Dynamic (b) Newmark-Beta. (c) Generalized alpha

(d) Multi-step Houbolt (e) Single step Houbolt

Fig 3. The von-mises stress contours at the initial time step of 1.6 μs.

The third time step is chosen at the end of the analysis where the analysis failed to converge to the required tolerance.

At the initial time interval (The starting time of the jump at the central axis)

In Fig 3. (a), the stress contours are obtained by solving the dynamic equations explicitly. The constant time steps are used in the explicit dynamic operator as there is no need for an adaptive time step during the analysis. The initial time step is 1.6 μs when the central point starts to rebound. In the explicit dynamic operator, the central point of the projectile does not rebound back as compared to other implicit schemes in which the central point starts lifting at a time

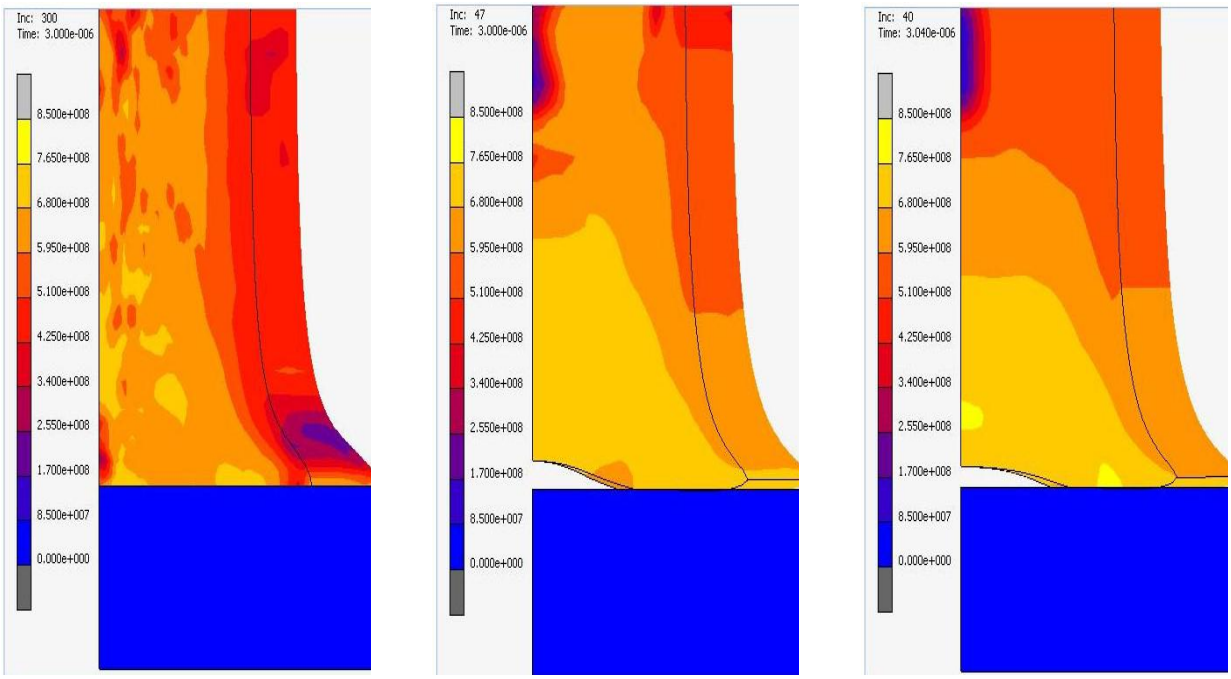

(a) Explicit Dynamic (b) Newmark-Beta. (c) Generalized alpha

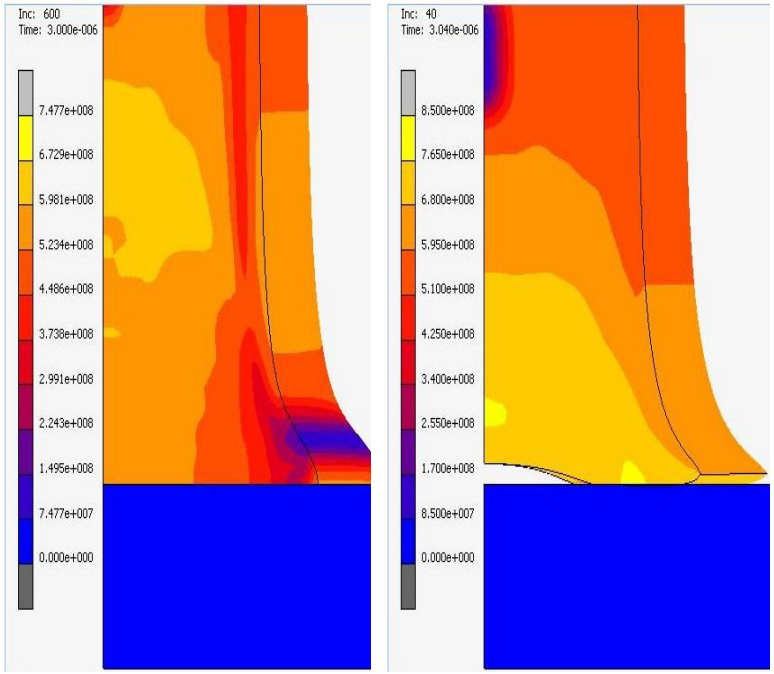

(d) Multi-step Houbolt (e) Single step Houbolt

Fig 4. The von-mises stress contours at the initial time step of 3.0 μs.

i.e., around 1.68 μs. The stress in the case of explicit dynamics is around 827 MPa. In Fig. 3(b), the solution is achieved by solving the Newmark-beta integration scheme. The stress distribution generated during the analysis is higher as compared to other solutions at the outer periphery of the rod. It happens because the outer edge bulges out after the initial stages of the impact. The lifting of the central point of the rod initiates at 1.60 μs. The Newmark dynamic operator at this initial stage is unconditionally stable with no numerical damping. In Fig 3(c), the stress distribution is obtained by solving equations using the second-order algorithm generalized alpha method. The maximum stress obtained by generalized alpha is around 850 MPa, which is consistent with the previous two distributions. The jump occurs at the

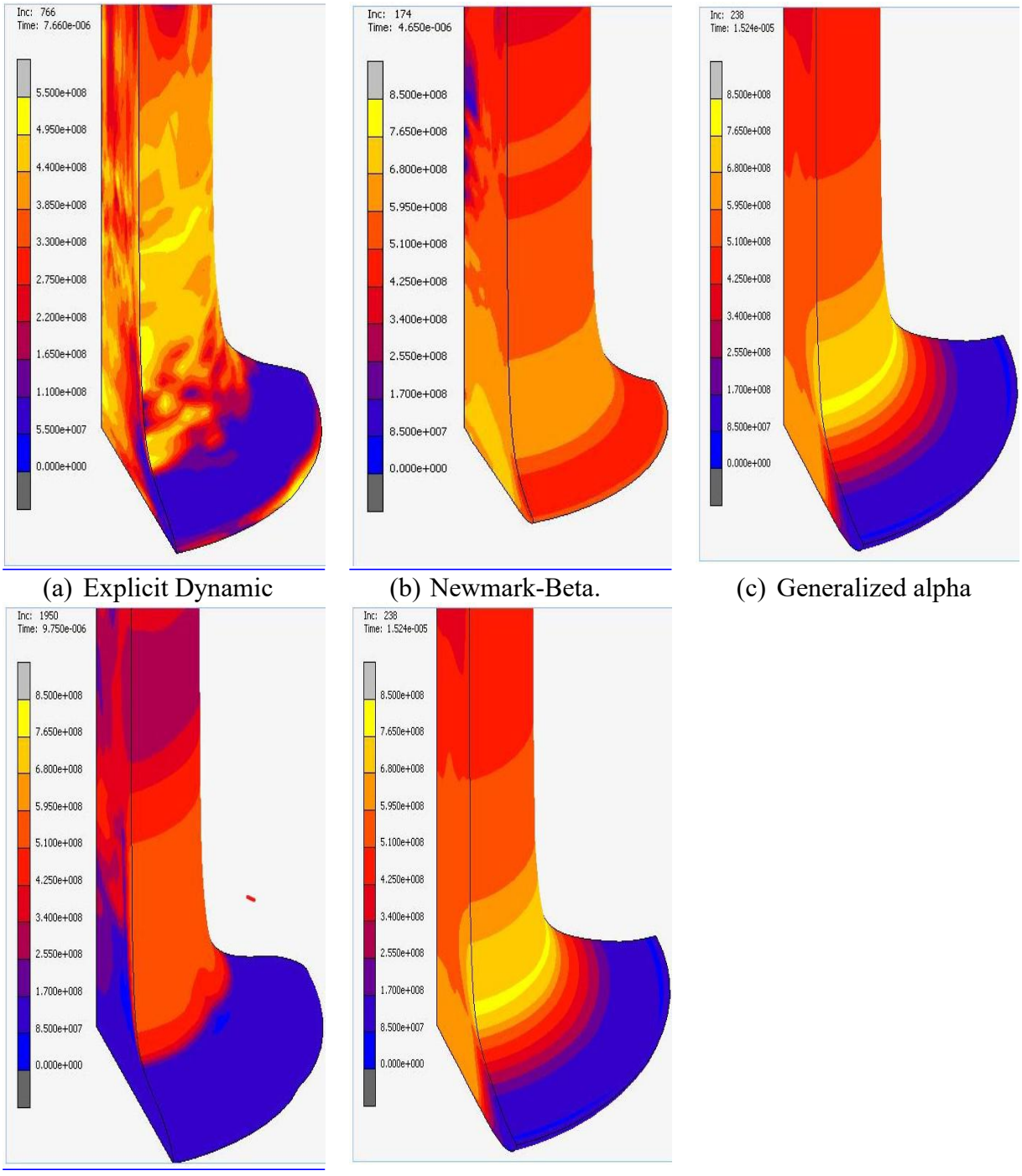

(a) Explicit Dynamic (b) Newmark-Beta. (c) Generalized alpha

(d) Multi-step Houbolt (e) Single step Houbolt

Fig 5. The von-mises stress contours at the initial time step of 3.0 μs.

central axis at around 1.6 μs. The single-step Houbolt algorithm can be treated as special cases of generalized-alpha algorithm. The stress distribution obtained in Fig. 3(e) by the single-step Houbolt algorithm is exactly similar due to the generalized-alpha distribution. The single-step generalized alphanumerical dissipation is controlled by two constant parameters α_f and α_m or by spectral radius. The generalized-alpha algorithm constant parameters comprise a number of other time integration algorithm. The equations which are solved using the generalized-alpha method $\alpha_f = 0$ and $\alpha_m = 1$ or spectral radius 0 are exactly similar to the stress distribution obtained by the single-step Houbolt algorithm. In Fig. 3(d) the stress distribution is obtained by solving time integrals by multistep Houbolt algorithm. The maximum stress

obtained is 850 MPa at the periphery of the outer edge of the Taylor rod while in other cases the maximum stress generated a little closer than the boundary of the Taylor rod. The jump at the central axis has not been observed in this case.

At the intermediate time interval (When the jump achieves the maximum distance at the central axis)

To analyze the effect of different time integration schemes on the stress distribution and the deformation behavior of the impact problem, it has become necessary to analyze the deformation/stress contour at different time intervals. The intermediate time interval in the present study is taken when the jump of the central point of the projectile achieves the maximum value. In the three integration schemes, the central point achieves maximum height at the time step of around 3.0 μs. As discussed in the previous section, in the explicit time integrations scheme there is no jump at the central axis of the projectile. The projectile remains in contact with the rigid target at the central point throughout the analysis as shown in Fig. 4(a). The outer edge of the projectile also remains in contact with the target. The deformation in the outer mushroomed part of the projectile is not similar to the deformation shown by Teng et al. [12]. The stress distribution is consistent with the literature, but the deformation pattern is not consistent. In the Newmark-beta algorithm the center portion lifts to 0.3 mm at 3.0 μs. The jump of the central portion is maximum as compared to other integration schemes. This represents the larger deformation of the projectile than the usual as shown in Fig. 4(b). For the Newmark integration operator, this will generate the requirement for the numerical damping to exclude the unnecessary numerical dissipation during the analysis.

The jump in the generalized-alpha scheme as well as in the single-step Houbolt operator as discussed earlier exhibits the same behavior as 0.2 mm while the jump in the multistep Houbolt operator has not been observed. The jump is considered to be an important factor in determining the stress and fracture pattern in the Taylor rod. When the jump-starts the triaxiality in the rod become positive which will in return increases the damage at the central axis of the rod. But the larger value of the jump in the case of the Newmark integration scheme is due to the uncontrolled numerical dissipation. The analysis will fail to achieve the required convergence in the later stages if the numerical dissipation is not controlled at the initial stages.

At the last time interval (Timestep where analysis failed to achieve the convergence)

In the last time step, the analysis is failed to achieve the required convergence. The maximum value of the stress in the explicit analysis is 550 MPa around the periphery of the projectile as shown in Fig. 5(a). The outer edge of the projectile lifts and this portion provide less resistance to the deformation as compared to the portion at the central axis or along the length of the rod. The stress distribution is nonlinear, generating the non-uniform stress distribution around the periphery of the rod as shown in Fig. 5(a). The analysis failed to achieve the required convergence at 7.0 μs. In the explicit dynamic integration, due to high-frequency dissipation, the excessive numerical damping has been introduced by the algorithm. This is the most likely reason for the response and non-occurrence of the jump in the rod using the dynamic operator. In Fig 5(b), the analysis failed to achieve the required convergence at 4.0 μs. The default parameters for the Newmark beta operators are $\beta = 0.25$ and $\gamma = 0.5$ as recommended by the literature failed to achieve the balance within 1 μs. The Newmark beta scheme implemented in the MSC Marc Mentat™ is not consistent with the default parameters. In the second study, the default parameters have been varied to $\beta = 0.5$ and $\gamma = 0.9142$. Using the Newmark integration scheme, the maximum time achieved by the analysis is 4.0 μs. The

stress contours are consistent with other integration schemes, but the analysis failed to achieve the prescribed tolerance. But the jump of the central point is also overpredicted, which represents the excessive numerical dissipation. In the study [16], the Newmark time integration scheme has been implemented to simulate the behavior of the Taylor rod impact problem. The algorithmic damping has been introduced in the study to analyze the Taylor rod impact problem. In the Newmark integration scheme, the incremental time is inversely proportional to the displacement and acceleration distribution. So, the dependence on the incremental time step leads to the instability of the structure. In Fig. 5(c), the analysis failed to converge up to the required tolerance at the time interval of 15 μs. The stress distribution is consistent with the literature. The maximum stress of 700 MPa is generated at the outer periphery of the projectile above the petal as shown in Fig. 5(c). The jump at the central point is also validated with the literature. The maximum von Mises stress is achieved at the central axis above the central point of the projectile. In Fig. 5(d), the stress distribution is similar to the Explicit dynamic analysis. The central axis as well as the outer periphery of the projectile remain in contact with the target throughout the analysis. No jump of the central axis has been observed using the multistep step Houbolt operator. In the multi-step Houbolt operator, the incremental time step is fixed during the analysis. The maximum stress in generated at the central axis as well at the outer periphery of the projectile. The stress is relieved as the outer edge of the rod lifts at the end of the analysis. As compared to the single-step Houbolt operator the multistep step Houbolt cannot be used with the adaptive time steeping which is necessary to capture the phenomenon of the impact process.

Conclusions

The numerical study of the Taylor rod has been performed to analyze the effect of different time integration schemes on the overall deformation behavior of the Taylor rod. The finite element method using MSC Marc Mentat™ is employed for this purpose. The triaxiality effect, Johnson-Cook plasticity, and stiffness reduction had been introduced in the study through an external Fortran-based user subroutine. The numerical results are validated with the experimental results. The effect of different integration schemes on the von-Mises stress distribution had particularly been discussed in the present work. The following conclusions have been drawn:

- The Explicit and Multi-step Houbolt operators coded in FE code MSC Marc Mentat™ are not able to capture the exact deformation in the Taylor rod impact test. The jump of the central point in the Taylor rod has not been observed in the aforementioned operators.
- In Explicit and Multistep Houbolt operators the central axis, as well as the outer edge of the rod remains in contact with the rigid wall throughout the analysis. The
- The Newmark-Beta operator in FE code MSC Marc Mentat™ overpredicts the deformation in the rod.
- The Newmark-beta operator exhibits excessive numerical dissipation. This results in the loss of accuracy, and this is the most likely reason for the overprediction of the deformation in Newmark integration.
- The WBZ time integration scheme can be treated as a special case of the single-step Houbolt operator and with parameters $\alpha_f = 0$ and $\alpha_m = 0$ the deformation is exactly similar to the Newmark-Beta integration scheme. If the parameters are fixed at $\alpha_f = 0$ and $\alpha_m = 0$, the deformation is exactly similar with the single-step Houbolt scheme.

- The Generalized-alpha method is the most suitable operator time integration operator to capture the exact deformation and stress distribution in the Taylor rod impact problem.

Acknowledgments

The support from the Council of Scientific Industrial Research (CSIR), New Delhi to carry out the present investigation in the form of a senior research fellowship is acknowledged.

References

[1] Taylor, G. (1948). The Use of Flat-ended Projectiles for Determining Dynamic Yield Stress, I: Theoretical Considerations, Proceedings of the Royal Society of London Series A. Mathematical and Physical Sciences, 194: 289–299.
[2] Chung, J. and Hulbert, G.M., "A family of single-step Houbolt time integration algorithms for structural dynamics", Comp. Meth. in App. Mech. Engg., 118, 1994.
[3] Chung, J. and Hulbert, G.M., "A time integration algorithm for structural dynamics with improved numerical dissipation: The Generalized-Method", Journal of Applied Mechanics, Vol. 60, pp. 371 - 375, June 1993.
[4] Hilber, H.M., Hughes, T.J.R., and Taylor, R.L., "Improved Numerical Dissipation for Time Integration Algorithms in Structural Dynamics", Earthquake Engineering and Structural Dynamics, Vol. 5, pp. 283-292, 1977.
[5] Newmark, N. M. "A Method of Computation for Structural Dynamics." ASCE of Eng. Mech. 85, 67-94, 1959.
[6] Wood, W.L., Bossak, M., and Zienkiewicz, O.C., "An Alpha Modification of Newmark's Method", International Journal for Numerical Methods in Engineering, Vol., 15, pp. 1562-1566, 1981.
[7] Chung, J. and Hulbert, G.M., "A time integration algorithm for structural dynamics with improved numerical
[8] Woodward, R.L., O'donnell, R.G. and Flockhart, C.J. (1992). Failure Mechanisms in Impacting Penetrators, Journal of Material Science, 27: 6411–6416.
[9] Worswick, M.J. and Pick, R.J. (1995). Void Growth and Coalescence During High Velocity Impact, Mechanics of Materials, 19: 293–309.
[10] Addessio, F.L., Johnson, J.N. and Maudlin, P.J. (1993). The Effect of Void Growth on Taylor Cylinder Impact Experiments, Journal of Applied Physics, 73: 7288–7297.
[11] Celentano, D.J. (2002). Thermomechanical Analysis of the Taylor Impact Test, Journal of Applied Physics, 91: 3675–3686.
[12] Teng, X., Wierzbicki, T., Hiermaier, S. and Rohr, I. (2005). Numerical Prediction of Fracture in the Taylor Test, International Journal of Solids and Structures, 42: 2929–2948.
[13] Bao, Y., Lee, Y., Wierzbicki, T. Evaluation and calibration of seven fracture models. International Journal of Mechanical Sciences, submitted.
[14] Gautam, S.S. and Saxena, R.K., 2012. A numerical study on effect of strain rate and temperature in the Taylor rod impact problem. The International Journal of Structural Changes in Solids, 4, pp.1-11.
[15] Gautam, S. and Saxena, R., 2015. A finite element study on effect of frictional heating in the Taylor rod impact problem. World Journal of Engineering.
[16] Gautam, S.S., Babu, R. and Dixit, P.M., 2011. Ductile fracture simulation in the Taylor rod impact test using continuum damage mechanics. International Journal of Damage Mechanics, 20(3), pp.347-369.
[17] Rathore, K.K., Jasra, Y. and Saxena, R.K., 2020. Numerical simulation of fracture behavior under high-velocity impact for Aluminium alloy 6060 target plate. Materials Today: Proceedings, 28, pp.1809-1815.
[18] Xiao, X., Mu, Z., Pan, H. and Lou, Y., 2018. Effect of the Lode parameter in predicting shear cracking of 2024-T351 aluminum alloy Taylor rods. International Journal of Impact Engineering, 120, pp.185-201.
[19] Iqbal, M.A., Senthil, K., Bhargava, P. and Gupta, N.K., 2015. The characterization and ballistic evaluation of mild steel. International Journal of Impact Engineering, 78, pp.98-113.
[20] MSC Software 2013 Volume A: Theory and user information (MSC. Software Corp.)
[21] Yadav, S., Singhal, S., Jasra, Y. and Saxena, R.K., 2020. Determination of Johnson-Cook material model for weldment of mild steel. Materials Today: Proceedings, 28, pp.1801-1808.